

Observed Antarctic Interannual Climate Variability and Tropical Linkages

DAVID P. SCHNEIDER, YUKO OKUMURA, AND CLARA DESER

Climate and Global Dynamics Division, Earth System Laboratory, National Center for Atmospheric Research, Boulder, Colorado*

(Manuscript received 7 May 2011, in final form 21 November 2011)

ABSTRACT

This study reviews the mechanisms associated with Antarctic–tropical climate linkages and presents new analyses of the seasonality and spatial patterns of tropical climate signals in the Antarctic for the late 1950s to the present. Tropical climate signals are primarily communicated to the Antarctic via the Pacific–South America (PSA) pattern and the southern annular mode (SAM). The impacts of these circulation patterns and their tropical linkages are evident in regressions of seasonally stratified Antarctic station temperature data and annually resolved ice core records on global fields of sea surface temperature, sea level pressure, and precipitation. Temperature and ice core anomalies in the Antarctic Peninsula region and adjoining areas of West Antarctica are significantly impacted by the PSA, interpreted as a Rossby wave train driven by anomalous tropical deep convection during ENSO events. This pattern is most evident in the austral spring, consistent with recent studies, suggesting that atmospheric conditions for Rossby wave propagation are most favorable during this season. During austral summer at the peak of the ENSO cycle, temperature anomalies at East Antarctic coastal stations exhibit significant correlations with tropical Pacific anomalies. This linkage reflects the influence of anomalous tropical heating on the position and strength of the subtropical jets and is consistent with changes in eddy momentum fluxes that alter the mean meridional circulation associated with the SAM. Of the ice cores that exhibit tropical linkages, most tend to be associated with the PSA teleconnection. The implications of the study’s findings for understanding Antarctic climate variability and climate change from seasonal to decadal time scales are also discussed.

1. Introduction

El Niño–Southern Oscillation (ENSO) arises from air–sea interactions in the tropical Pacific Ocean and is widely considered to be the dominant source of global climate variability on interannual to decadal time scales (e.g., Trenberth et al. 1998; Neelin et al. 1998; Zhang et al. 1997). The presence of ENSO signals in the high-latitude Southern Hemisphere (SH) in a variety of variables has been recognized for some time (e.g., Trenberth 1975; Mo and White 1985; Savage et al. 1988; Karoly 1989), but the associated teleconnection patterns and their impacts are not widely appreciated. Given evidence that changes in tropical climate are influencing

trends in Antarctic temperature, sea ice (Ding et al. 2011; Schneider et al. 2012), and possibly the ice sheet itself (Steig et al. 2012), it is important to place our understanding of Antarctic–tropical linkages on firmer ground than has been previously possible (Turner 2004).

A well-known ENSO teleconnection pattern is the Pacific–North America (PNA) pattern (e.g., Wallace and Gutzler 1981). Although the PNA can vary independently of ENSO, the Rossby wave-forcing generated by ENSO events projects onto the PNA. An El Niño event is associated with the positive phase of the PNA pattern, characterized by a deep Aleutian low, high pressure over western Canada, and low pressure anomalies over the southern tier of the United States (e.g., Wallace and Gutzler 1981).

The SH’s counterpart to the PNA is the Pacific–South America (PSA) pattern (e.g., Ghil and Mo 1991; Mo and Higgins 1998; Mo 2000). Some authors have described two PSA patterns in quadrature as being part of a propagating wave that can be excited by anomalous tropical convection (e.g., Mo and Higgins 1998; Mo and Paegle

* The National Center for Atmospheric Research is sponsored by the National Science Foundation.

Corresponding author address: David P. Schneider, Climate and Global Dynamics Division, Earth System Laboratory, National Center for Atmospheric Research, Box 3000, Boulder, CO 80307-3000.
E-mail: dschneid@ucar.edu

2001), though others view the PSA patterns as geographically fixed standing waves that are only correlated with ENSO-related tropical convection anomalies in austral spring (Robertson and Mechoso 2003). The first PSA pattern is characterized as a wave train extending from New Zealand across the South Pacific to southern South America. The second PSA pattern has a characteristic zonal wave-3 structure over the Southern Ocean (Mo and Higgins 1998). As we will show, the first PSA pattern comes out directly through regressions of atmospheric circulation data upon tropical indices [e.g., the Southern Oscillation index (SOI)]; it is also the main feature in the SH of circulation anomalies for composites of El Niño or La Niña events (e.g., Deser et al. 2010). Therefore, we focus only on the first PSA pattern, in accordance with the view that it is the main response to ENSO in the SH extratropics on the interannual time scale (e.g., Mo and Paegle 2001).

This paper also highlights the significant interactions of the southern annular mode (SAM) and ENSO activity (e.g., Seager et al. 2003; L'Heureux and Thompson 2006; Fogt et al. 2011), and their importance to Antarctic temperature anomalies in the austral summer. The SAM is a seesaw of atmospheric mass between the mid- and high latitudes of the SH (e.g., Thompson et al. 2000; Fogt and Bromwich 2006). The recognition that the SAM is linked with ENSO variability is relatively new; although Karoly (1989) described a SAM-like zonally symmetric structure in the austral summer atmospheric circulation anomalies associated with ENSO events, he linked this to Rossby wave forcing. However, Seager et al. (2003) promoted a new hypothesis that ENSO variability influences the extratropical atmospheric circulation via a mechanism distinct from a Rossby wave train. This alternative mechanism involves eddy-mean flow interactions and associated anomalies in the zonally symmetric circulation driven by anomalous heating throughout the troposphere in the tropics. As discussed below, other studies have since refined this idea (e.g., Seager et al. 2005, 2010; L'Heureux and Thompson 2006; Fogt et al. 2011). We present corroborating evidence that this mechanism is real and that it has a significant influence on temperature anomalies over Antarctica.

Concerns have been raised about the strength and consistency of ENSO teleconnections over Antarctic and the Southern Ocean (e.g., Turner 2004; Cullather et al. 1996; Fogt and Bromwich 2006; Gregory and Noone 2008). Composites of seasonal mean atmospheric circulation anomalies indicate that ENSO teleconnections are present year-round in the Pacific sector of the Antarctic (e.g., Trenberth and Caron 2000; Deser et al. 2010). However, the circulation patterns exhibit significant changes in strength and shape in different seasons,

and may be different from one event or decadal epoch to the next (e.g., Turner 2004; Cullather et al. 1996; Fogt and Bromwich 2006; Gregory and Noone 2008). The apparent instability or weakness of ENSO-related circulation anomalies in the Antarctic has been partly attributed to the relative dominance of the SAM. It is common in analyses of SH atmospheric circulation anomalies to treat the SAM and PSA patterns as distinct modes with their own time scales and physics (e.g., Mo 2000; Cai and Watterson 2002). Indeed, the SAM and PSA patterns are often defined as the first and second empirical orthogonal functions (EOFs) of SH geopotential height or sea level pressure (SLP) anomalies, respectively (Mo 2000; Cai and Watterson 2002; Schneider et al. 2004). The SAM is an intrinsic mode of atmospheric variability (e.g., Limpasuvan and Hartmann 2000) and as such can vary independently of ENSO.

Part of the apparent inconsistency of the PSA pattern in association with ENSO events may be attributed to the seasonality of the SH atmospheric circulation, which has largely not been considered in previous studies of ENSO teleconnections in Antarctica and the Southern Ocean. For example, the subtropical and polar front jets change in their relative positions and strengths (e.g., Bals-Elsholz et al. 2001; Williams et al. 2007), which has implications for the interactions of Rossby wave energy with the storm tracks. An interesting observation is that although the peak amplitude of ENSO-related tropical SST anomalies occurs in the austral summer [December–February (DJF)], the peak amplitude of the PSA anomalies during ENSO episodes occurs in the austral spring [September–November (SON); e.g., Jin and Kirtman 2009]. The analysis of Jin and Kirtman (2009) showed that the SH Rossby wave source is strongest in the austral spring and abruptly weakens in the austral summer. Therefore, the primary SH response to ENSO—namely, the PSA wave train—precedes the peak amplitude of SST anomalies in the tropical Pacific by about one season. In support of this hypothesis, Mo (2000) showed the PSA pattern to be most significantly correlated with tropical SSTs in the austral spring. In modeling experiments with ENSO forcing shifted by 6 months, the NH response preceded ENSO peak forcing, suggesting that the extratropical patterns forced by ENSO depend on the seasonality of the extratropical atmosphere (Jin and Kirtman 2009).

Describing a second mechanism of tropical–extratropical linkages, Seager et al. (2003) argued that during an El Niño event, anomalous tropical heating strengthens the meridional temperature gradient, enhancing the subtropical jets, which act as waveguides to steer transient eddies on a more equatorward and zonal path than in the climatological mean flow. Associated with the equatorward

TABLE 1. Names of locations corresponding to labels in Fig. 2. Boldface names indicated records used for the one-point regression maps in Figs. 4, 5, 8, and 9. Parentheses in the stations section list start year of record as used in this study, latitude, and longitude. Parentheses in the ice cores section list end year of the record as used in this study, latitude, and longitude.

Stations
1. Amundsen–Scott South Pole (1958; 90°S, 0°W)
2. Novolazarevskaya (1961; 70.8°S, 11.8°E)
3. Syowa (1966; 69.0°S, 39.6°E)
4. Mawson (1958; 67.6°S, 62.9°E)
5. Davis (1958; 68.6°S, 78.0°E)
6. Mirny (1958; 66.5°S, 93.0°E)
7. Vostok (1958; 78.5°S, 106.9°E)
8. Casey (1959; 66.3°S, 110.5°E)
9. Dumont D’Urville (1958; 66.7°S, 140.0°E)
10. Scott Base (1958; 77.9°S, 166.7°E)
11. Rothera (1977; 67.5°S, 68.1°W)
12. Faraday (1958; 65.4°S, 64.4°W)
13. O’Higgins (1963; 63.3°S, 57.9°W)
14. Esperanza (1958; 63.4°S, 57.0°W)
15. Marambio (1971; 64.2°S, 56.7°W)
16. Orcadas (1958; 63.3°S, 44.7°W)
17. Halley (1958; 75.5°S, 26.4°W)
18. Neumayer (1982; 70.7°S, 8.4°W)
Ice cores
A. Dronning Maud Land (1997; 70.66°S, 0°E)
B. Vostok snow pit (1999; 78.0°S, 106°E)
C. Law Dome 2000 (1999; 66.78°S, 112.82°E)
D. Talos Dome (1996; 72.8°S, 159.75°E)
E. Siple Dome A (1993; 81.65°S, 148.81°W)
F. ITASE 00–5 (1999; 77.68°S, 123.99°W)
G. ITASE 00–1 (1999; 79.38°S, 111.23°W)
H. ITASE 02–4 (1999; 86.5°S, 107.99°W)
I. ITASE 01–2 (1999; 77.84°S, 102.91°W)
J. ITASE 01–3 (1999; 78.12°S, 95.65°W)
K. ITASE 01–5 (1999; 77.06°S, 89.14°W)
L. Siple station (1983; 75.92°S, 84.15°W)
M. Gomez (1980; 74.02°S, 70.63°W)
N. Dyer Plateau (1989; 70.66°S, 64.5°W)
O. Dolleman Island (1981; 60.5°S, 70.30°W)
P. James Ross Island (1999; 64.2°S, 57.67°W)
Q. Berkner Island (1990; 79.61°S, 45.72°W)

shift in the storm track, anomalous ascent occurs over the midlatitudes, causing cooling, while descent occurs at polar latitudes, causing warming. L’Heureux and Thompson (2006) described variations on this mechanism and found a significant relationship between the SAM and SST anomalies associated with ENSO in the eastern equatorial Pacific for November–February. Their work implied that a negative SAM phase, or higher pressure over the Antarctic, is associated with a warm ENSO event, consistent with the equatorward shift of the storm tracks described by Seager et al. (2003, 2005, 2010).

To explain SAM–ENSO correlations, Fogt et al. (2011) investigated the relative phasing of SAM and

ENSO events and associated anomalous poleward eddy momentum fluxes. Although supporting the general arguments of Seager et al. (2003, 2005) and L’Heureux and Thompson (2006), Fogt et al. (2011) also suggested that in certain combinations of positive and negative SAM and ENSO phases, the eddy momentum fluxes associated with SAM and ENSO can be opposing, weakening the high-latitude ENSO signal. However, the occurrence of opposing eddy momentum fluxes has a seasonal dependence, occurring more often in austral winter and early spring, while strong, reinforcing interactions tend to occur more often in November–February (Fogt et al. 2011). The impacts of the ENSO modulation of the SH zonally symmetric circulation have not been widely discussed.

The primary contribution of this study is providing a concise description of the seasonality and spatial patterns of tropical signals in the Antarctic, with a view toward a better physical understanding of observed Antarctic interannual climate variability in the context of the dynamical mechanisms discussed in previous work (Seager et al. 2003; L’Heureux and Thompson 2006; Jin and Kirtman 2009; Fogt et al. 2011). Our focus is the period from the late 1950s to the present, representing the era of continuous meteorological records from Antarctic research stations (e.g., Turner et al. 2004). We first present an overview of atmospheric anomalies related to indices of SAM and ENSO variability, followed by a survey of teleconnections associated with one-point regression maps of Antarctic station records, and discuss the consistency of the two approaches. The zonal symmetry of the tropical teleconnection in austral summer is then further explored using reanalysis data to show that the surface signals in the Antarctic are coherent with circulation anomalies throughout the troposphere from the tropics to the Antarctic. Additionally, we compare tropical linkages evident in Antarctic meteorological records with those in ice core records over the course of the instrumental era, so that ice core records may be better applied to extending the knowledge of Antarctic–tropical linkages prior to the instrumental era.

2. Data and methods

a. Antarctic data

For Antarctic observational data, we use monthly-mean observations of surface air temperature (SAT) from the Reference Antarctic Data for Environmental Research (READER) archive (Turner et al. 2004). As indicated in Table 1, the majority of the 18 station records we select have nearly complete records from 1958 to present. In the case of missing data, the missing years or

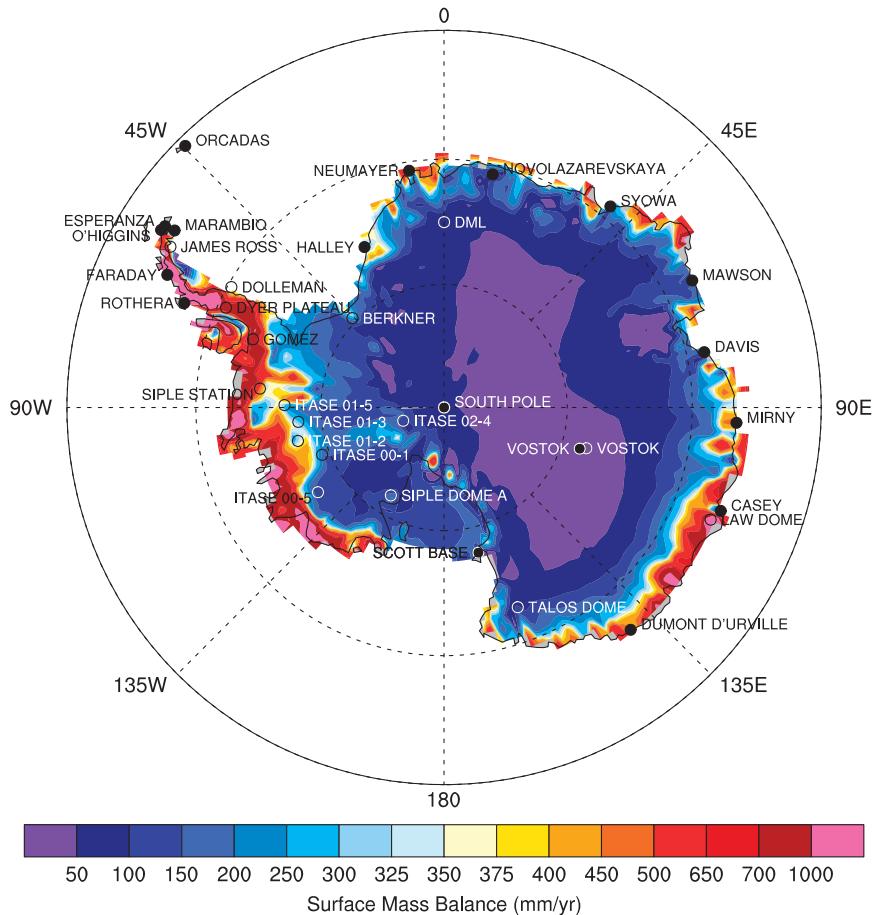


FIG. 1. Map of the Antarctic study region. Locations of long-term monthly SAT records from the READER archive are marked by solid black circles. Locations of annual ice core records discussed in the text are indicated as open black or white circles. Background color scale is the annual mean surface mass balance (mm, water equivalent per year) from van de Berg et al. (2006), as provided by A. Monaghan and used with permission.

seasonal means are not included in the regressions discussed below. The station data were downloaded in early 2010 (from <http://www.antarctica.ac.uk/met/READER/data.html>). The monthly index of the SAM is used from Marshall (2003) and was obtained online (at <http://www.antarctica.ac.uk/met/gjma/sam.html>).

Knowledge of ENSO signals in the high latitudes of the SH has been hampered in part by the short duration and sparseness of the observational network. Annually or subannually resolved ice cores (e.g., Steig et al. 2005) present a valuable opportunity to address the observational gaps. ENSO signals in Antarctic ice core records have been reported by several studies (e.g., Bromwich et al. 2000; Ichayanagi et al. 2002; Schneider and Steig 2008; Gregory and Noone 2008; Divine et al. 2009; Naik et al. 2010). Here, we use the Antarctic set of annual mean ice core records of water isotopes ($\delta^{18}\text{O}$ and δD), generally a proxy for temperature, that were compiled

and evaluated by Schneider and Noone (2007) and described in references therein. Two additional records, provided by Dr. R. Mulvaney of the British Antarctic Survey, are from Gomez and Dolleman Island (Peel et al. 1988). Figure 1 indicates the locations of station and ice core records. As indicated on Table 1, the records have various ending dates; most end in 1999 but several end in the 1980s. All of the ice core records go back to the 1958 start year of our analysis. The original ice core time series of water isotope data ($\delta^{18}\text{O}$ or δD) are used in standardized form for the purposes of this study.

Although ice core records significantly broaden the spatial coverage and temporal length of Antarctic climate datasets, there remain ambiguities in their interpretation because of the reliance on annual data, uncertainties in dating, seasonality of deposition, and multiple physical controls on isotopic fractionation (e.g., Masson-Delmotte et al. 2008). Our approach to understanding these records

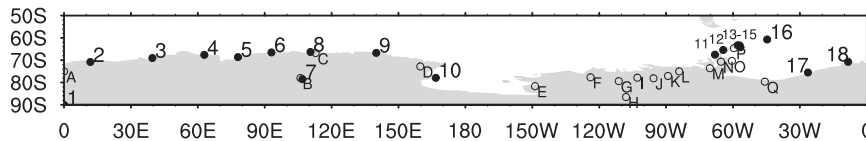


FIG. 2. Reference map indicating the locations of station records (numbered, solid circles) and ice core records (letters, open circles) corresponding to the names in Table 1.

is through direct comparison with station data. It has been suggested (Turner 2004) that ice core records are only useful for climate studies after a certain amount of low-pass smoothing because of low snow deposition rates in the Antarctic. However, as illustrated in Fig. 1, the annual surface mass balance (precipitation minus sublimation and snowmelt; van de Berg et al. 2006) varies considerably across the Antarctic continent. In general, annual ice core time series can be recovered where the snow accumulation exceeds 100 mm yr^{-1} ; this includes essentially all of West Antarctica and Law Dome in East Antarctica. The dating uncertainty tends to be lower for higher accumulation rate cores and the amount of material persevered is greater, potentially enhancing the climate signal that is preserved.

b. Global and tropical data

We compute one-point, least squares regression and correlation maps using a globally complete, $2^\circ \times 2^\circ$ latitude–longitude gridded dataset of SST anomalies known as the National Oceanic and Atmospheric Administration’s (NOAA) Extended Reconstructed SST, version 3b (ERSSTv3b) (Smith et al. 2008), and a globally complete, $5^\circ \times 5^\circ$ latitude–longitude gridded dataset of SLP, the Hadley Centre SLP, version 2 (HadSLP2; Allan and Ansell 2006). Both gridded datasets have monthly resolution, span the main 1958–2008 period of our analyses, and were obtained from the Physical Science Division of the NOAA Earth System Research Laboratory in Boulder, Colorado (<http://www.esrl.noaa.gov/psd/data/>). Prior to computing the regression maps, the local monthly climatology was subtracted from each grid point for a common base period, and the local least squares linear trends were removed from the resulting monthly anomaly time series. Then, the SST or SLP anomalies were spatially smoothed with a local nine-point filter to reduce the small-scale noise in the regression patterns. The Antarctic in situ SAT data are treated in the same manner but with no spatial smoothing.

Additionally, we compute regressions or correlations of Antarctic time series with two precipitation datasets; a dataset of land station precipitation (Hulme et al. 1998), provided on a $2.5^\circ \times 3.75^\circ$ latitude–longitude grid with no interpolation or infilling; and a global gridded dataset, the Global Precipitation Climatology Project,

version 2.1 (GPCP) (Adler et al. 2003), obtained from the National Center for Atmospheric Research (NCAR) (http://www.cgd.ucar.edu/cas/catalog/satellite/gpcp/gpcp_v21.html). The Hulme et al. (1998) network of stations is relatively sparse, but it provides longer temporal coverage than the GPCP, which only covers 1979–present.

We calculate a standardized SOI from the HadSLP2 data, subtracting the area-averaged SLP anomalies between 20°N and 20°S and all longitudes except 180° – 80°W (“Darwin”) from those between 20°N and 20°S and 180° and 80°W (“Tahiti”). Results are very similar using the SOI of Trenberth (1984). Similarly, we use the SST data to compute the Niño-3.4 index as the area-averaged SST anomaly in the region 5° – 5°S , 120° – 170°W . Additional data include three-dimensional temperature and zonal mean wind fields from the National Centers for Environmental Prediction, version 2 (NCEP2), reanalysis for 1979–2008 (Kanamitsu et al. 2002), obtained from the NOAA Earth System Research Laboratory (<http://www.esrl.noaa.gov/psd/data/gridded/>).

To illustrate the organized spatial patterns associated with Antarctic temperature or ice core anomalies, our regression maps show the entire field of regression values. Our discussion and interpretations are focused on features that are robust and consistent across several physical variables (e.g., SST, SLP, precipitation). Statistical significance is assessed using a two-tailed t test, and significant ($p < 0.05$) regression values in the SST field are indicated in the regression maps by white stippling. Because of the sometimes limited overlap between the ice core data and the Hulme et al. (1998) precipitation data, an additional requirement was imposed that the sample size be at least 20 values. Figure 2 indicates the locations of the Antarctic ice core and station data using the same map projection as the regression maps; Table 1 lists the corresponding names and latitude–longitude information.

3. Results

a. Comparison of SAM and ENSO signals

We examine the spatial patterns of anomalies in SLP, SST, precipitation, and Antarctic station SAT and ice core records associated with one standard deviation of

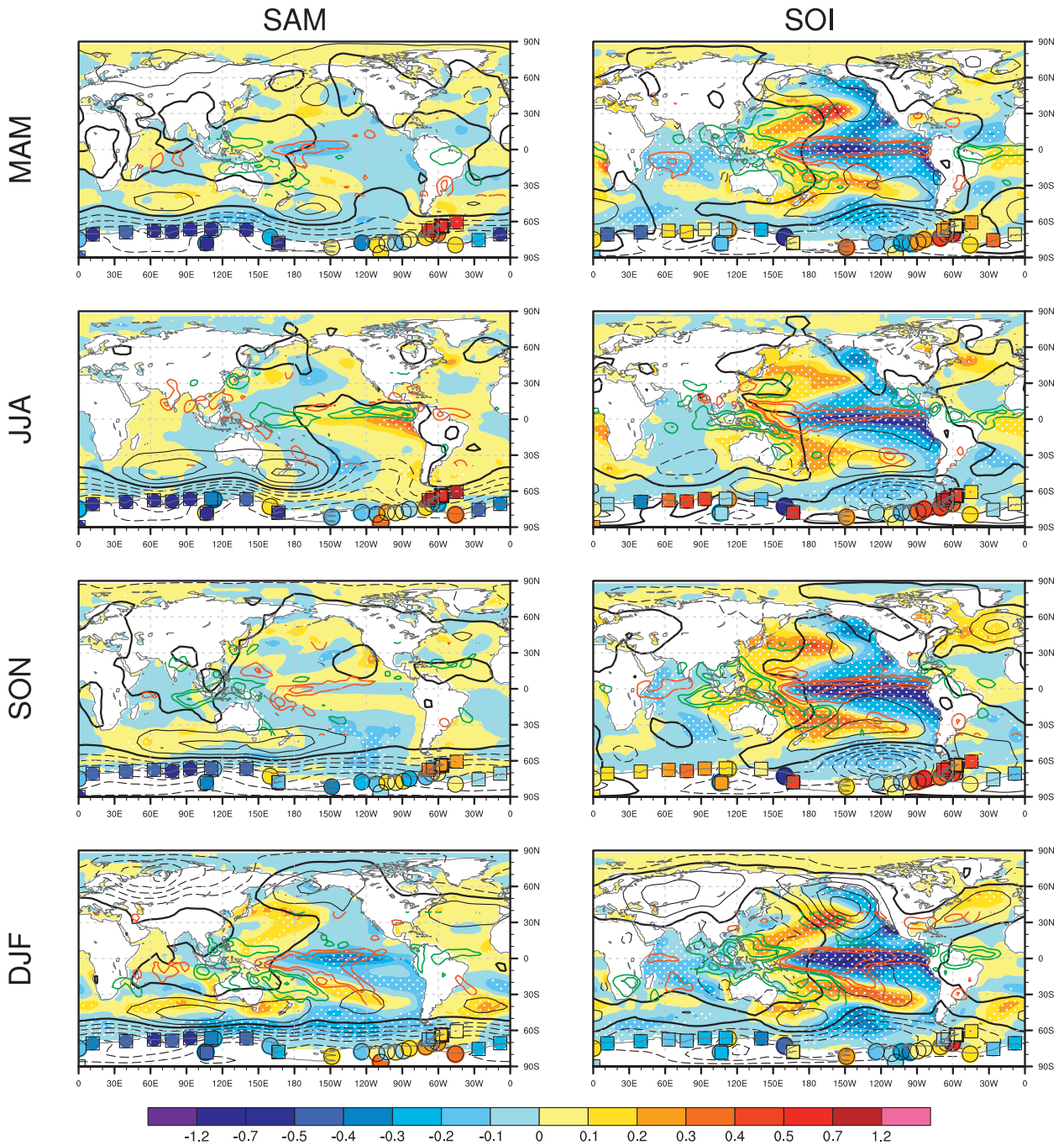


FIG. 3. Regressions of seasonal mean anomalies of SST (1958–2008; gridded colors, °C per standard deviation), SLP (1958–2008; black contours, hPa per standard deviation; positive values solid and negative values dashed, interval of 0.4 hPa; white stippling indicates values of at least the 95% significance level), GPCP precipitation (1979–2008; green and orange contours for positive and negative precipitation anomalies, respectively; lines drawn at $-1.2, -0.6, -0.3, 0.3, 0.6, 1.2 \text{ mm day}^{-1}$) and Antarctic station data (1958–2008; squares, °C per standard deviation) upon corresponding (top to bottom) seasonal mean (left) SAM and (right) SOI indices. Also shown are correlations of the seasonal SAM and SOI indices with the annual ice core anomalies (generally 1958–99; circles, units of correlation coefficients).

the SAM and SOI in each season in Fig. 3. Similar results are obtained using alternative indices of ENSO variability, such as the Niño-3.4 index, and from composite analysis (not shown). Throughout the year, the SAM is

associated with a zonally symmetric pattern of negative SLP anomalies over the high-latitude SH and positive SLP anomalies in the midlatitudes. The zonal symmetry is most pronounced in SON and DJF, being interrupted

in the midlatitude eastern Pacific sector in March–May (MAM) and June–August (JJA).

The characteristic “cold continent–warm peninsula” pattern associated with the positive phase of the SAM (Schneider et al. 2006) is clearly evident in the SAT dataset. At coastal East Antarctica stations, SAT anomalies in excess of -0.8°C occur in MAM and JJA, contrasted with anomalies greater than $+0.7^{\circ}\text{C}$ in the western Antarctic Peninsula. Weaker anomalies and a less-pronounced spatial contrast occur in SON and DJF; East Antarctic coastal anomalies range from -0.2° to -0.6°C , and only the northernmost Antarctic Peninsula stations show positive temperature anomalies, in the range of $+0.1$ to $+0.3^{\circ}\text{C}$. The sign of the adjacent SST anomalies is consistent with the Antarctic coastal stations, and the values are most significant in DJF. However, it should be noted that the SST dataset does not include air temperature anomalies over sea ice, which would be expected to have anomalies of larger magnitude than SSTs (e.g., Yuan and Li. 2008; Kwok and Comiso 2002). Individual ice core isotopic records are not strongly correlated with the SAM: the largest correlations are in the range of 0.3–0.4 at the Berkner Island and International Trans-Antarctic Scientific Expedition (ITASE) 02–4 sites. Similar values are obtained using annual indices for the correlations—only the values at Dronning Maud Land (DML) and ITASE 00–5 improve by about 0.1 compared to their maximum seasonal values (not shown).

For SLP, precipitation, and SST anomalies in the low and midlatitudes, the patterns associated with the SOI, on the right column of Fig. 3, are consistent with those shown in previous work associated with the Southern Oscillation (e.g., Trenberth and Caron 2000) and with composites of El Niño and La Niña events (e.g., Deser et al. 2006, 2010). The circulation pattern in the SH extratropics strongly resembles the PSA 1 of Mo (2000); as such, we use the term “PSA pattern” to refer to this ENSO teleconnection. The PSA is associated with significant SST anomalies in the South Pacific in all seasons. As drawn, the maps exemplify La Niña conditions. Specifically, in the tropics, the SOI is associated with an east–west seesaw of SLP with nodes near the date line and $\sim 60^{\circ}\text{W}$ over South America. The largest east–west pressure contrast occurs in DJF when the pressure anomalies are also most symmetric about the equator. The largest tropical SST anomalies are located along the equatorial central and eastern Pacific, with the anomalies becoming progressively stronger from MAM through DJF. Opposite-signed SST anomalies of somewhat weaker amplitude than the central and eastern equatorial Pacific anomalies occur in the western Pacific basin. The precipitation anomalies over the Pacific basin

and Indonesia largely follow the underlying SST anomalies. In all seasons, reduced precipitation is evident along the equator from about 150°E to 90°W , while increased precipitation is evident over Indonesia and northern Australia. The spatial extent of the precipitation anomalies is largest in DJF.

The patterns described above provide a guide for interpreting the linkages of the SAM with tropical variability, which are also evident in Fig. 3. The most widespread and significant anomalies in the tropics associated with the SAM are in DJF. Specifically, for the positive SAM phase, tropical rainfall is generally reduced from 150°E to 90°W and increased over Indonesia and the South Pacific convergence zone (SPCZ). The rainfall anomalies are physically consistent with the underlying SST patterns and also with the low-level wind convergence implied by the SLP distribution. Weaker rainfall anomalies with the same sign as those in DJF are evident in SON and MAM but opposite in sign during JJA.

The PSA pattern exhibits a seasonal evolution. In all seasons, there is a low pressure anomaly in the South Pacific from approximately 150° to 60°W , with a center at approximately 110°W , between 60° and 70°S . The strength of the center increases from 1.6 hPa in MAM and JJA to 2 hPa in SON, and decreases to 1.2 hPa in DJF. The weakening of the center from SON to DJF is associated with a change in the shape of the circulation anomaly, from a regional feature to a more hemispheric and zonally symmetric pattern. The weakening of the teleconnection occurs despite the increase of the equatorial SST and rainfall anomalies from SON to DJF.

The impacts of the teleconnection on Antarctic temperature and ice core records also show a seasonal evolution. Consistent with the cyclonic circulation anomaly in the South Pacific, positive anomalies occur from 90° to 60°W and negative anomalies occur from 130° to 100°W , in a pattern resembling the Antarctic dipole (e.g., Yuan and Martinson 2000; Renwick 2002). The strength of the anomalies changes with the seasons, particularly in the 90° – 50°W sector. SAT anomalies at the Faraday and Rothera stations on the Antarctic Peninsula, for example, are only 0.2° – 0.4°C in MAM but nearly 0.7°C in SON and greater than 1°C in JJA. Three ice core records in this sector (Gomez, Siple station, and ITASE 01–5) have correlations of $r > 0.4$ with the SOI in SON.

The change in the nature of the teleconnection from SON to DJF is accompanied by a change in the sign of East Antarctic SAT anomalies (10° – 150°E) with respect to the SOI. In addition, the negative pressure anomalies over East Antarctica increase in strength, and the adjacent SST anomalies increase in magnitude and significance. The result is that the anomalies associated with the SOI in DJF resemble those associated with the

SAM, suggesting a coupling of the SAM with ENSO variability in the austral summer. The two spatial patterns (bottom row of Fig. 3) are consistent with SAM–ENSO correlations found in previous work (e.g., Carvalho et al. 2005; L’Heureux and Thompson 2006). Ciasto and Thompson (2008) also found a mimicking of SAM and ENSO signatures in the austral summer for the high-latitude SST and geopotential height fields.

b. One-point correlation maps using station data

The one-point regression maps in Figs. 4 and 5 show the amplitude and sign of SST, SLP, and low-latitude precipitation anomalies associated with SAT anomalies at eight individual Antarctic stations (marked by black squares), including the Antarctic Peninsula region and Scott Base in Fig. 4 and the South Pole and three East Antarctic coastal stations in Fig. 5. The regressions in Figs. 4 and 5 are arranged horizontally in an eastward direction from Scott Base and vertically by seasonal means. This view highlights remarkable regional and seasonal variability in the teleconnection patterns, pursuant to the idea that Antarctic–tropical linkages are highly seasonally and regionally dependent. To gain an understanding of the representativeness of each station, correlations of the selected individual stations with anomalies at all of the other stations and ice core records are also shown.

From MAM to SON, SH circulation anomalies associated with the stations in Fig. 4 resemble the PSA pattern, with some shifting in the longitude of the maximum pressure anomaly from west to east depending on the station. The closest match of the one-point regression maps with the SOI-related patterns (Fig. 3) occurs during SON in association with SAT anomalies at Faraday. SST, SLP, and rainfall anomalies over the tropical Pacific and Indian Oceans are markedly similar whether the SOI or the Antarctic station data are used to compute the regression maps. Specifically, warm anomalies in the western Antarctic Peninsula region occur in association with increased rainfall across Indonesia, eastern Australia, and the SPCZ, decreased rainfall in the central equatorial Pacific, positive SST anomalies in the western Pacific, and negative SST anomalies in the eastern equatorial Pacific, along the western margins of North and South America, and in the western Indian Ocean. The overall pattern in the SH can be interpreted as indicative of a Rossby wave originating from the western Pacific or SPCZ, impacting temperature anomalies in the Antarctic Peninsula region through atmospheric thermal advection.

The tropically forced teleconnection appears to abruptly cease from SON to DJF, when Faraday no longer exhibits a significant relationship with tropical SSTs. For Orcadas

station, however, associated tropical precipitation and SST anomalies strengthen from SON to DJF, in association with a shift in the circulation pattern from a cyclonic to a more zonal pattern. Temperature anomalies at Orcadas station tend to be anticorrelated with those at East Antarctic stations in all seasons of the year, indicative of a relationship between Orcadas SAT and the SAM. By contrast, SAT anomalies at Faraday do not always show significant relationships with the SAM (e.g., Marshall et al. 2006).

One-point regression maps using the South Pole and coastal East Antarctic station data (Fig. 5) exhibit markedly different patterns than the Antarctic Peninsula maps. In all seasons, the patterns using these stations resemble the SAM patterns with opposite sign, and the strongest zonal symmetry of the SLP patterns occurs during DJF. SAT anomalies at East Antarctic stations are highly coherent with each other; for example in DJF anomalies at Davis are correlated at $r > 0.7$ with anomalies at the seven other stations from 10° to 150° E. In MAM and JJA, the contrasting pattern of opposite-signed anomalies between the western Antarctic Peninsula and coastal East Antarctica is evident, with positive anomalies at Novolazarevskaya, Davis and Dumont D’Urville opposing anomalies at Rothera, Faraday, Esperanza and Orcadas. The East Antarctic stations have relatively weak relationships with anomalies in the ice cores scattered across West Antarctica.

In contrast to the lack of tropical linkages around the western Antarctic Peninsula in DJF, SAT anomalies at East Antarctic coastal stations are related to positive SST and rainfall anomalies in the central and eastern tropical Pacific, and negative SST and rainfall anomalies in the western Pacific, as well as an anomalously deep Aleutian low (Fig. 5). Remarkably, the tropical rainfall anomalies associated with positive SAT anomalies in East Antarctica are nearly opposite those associated with positive SAT anomalies at Orcadas, suggestive of a systematic alteration of the SAM associated with ENSO variability.

c. Zonal symmetry of tropical linkages in DJF

Important to the interpretation of the coupling behavior of ENSO and the SAM is the vertical structure of temperature and zonal wind anomalies associated with these two phenomena. L’Heureux and Thompson (2006) showed that SH tropospheric zonal wind anomalies associated with SSTs in the eastern equatorial Pacific (the cold tongue region) resemble those associated with the SAM index, suggesting that the SAM captures most of the extratropical response to ENSO in the austral summer. Does the SAM response to ENSO, which involves the zonal mean circulation, impact the surface climate of

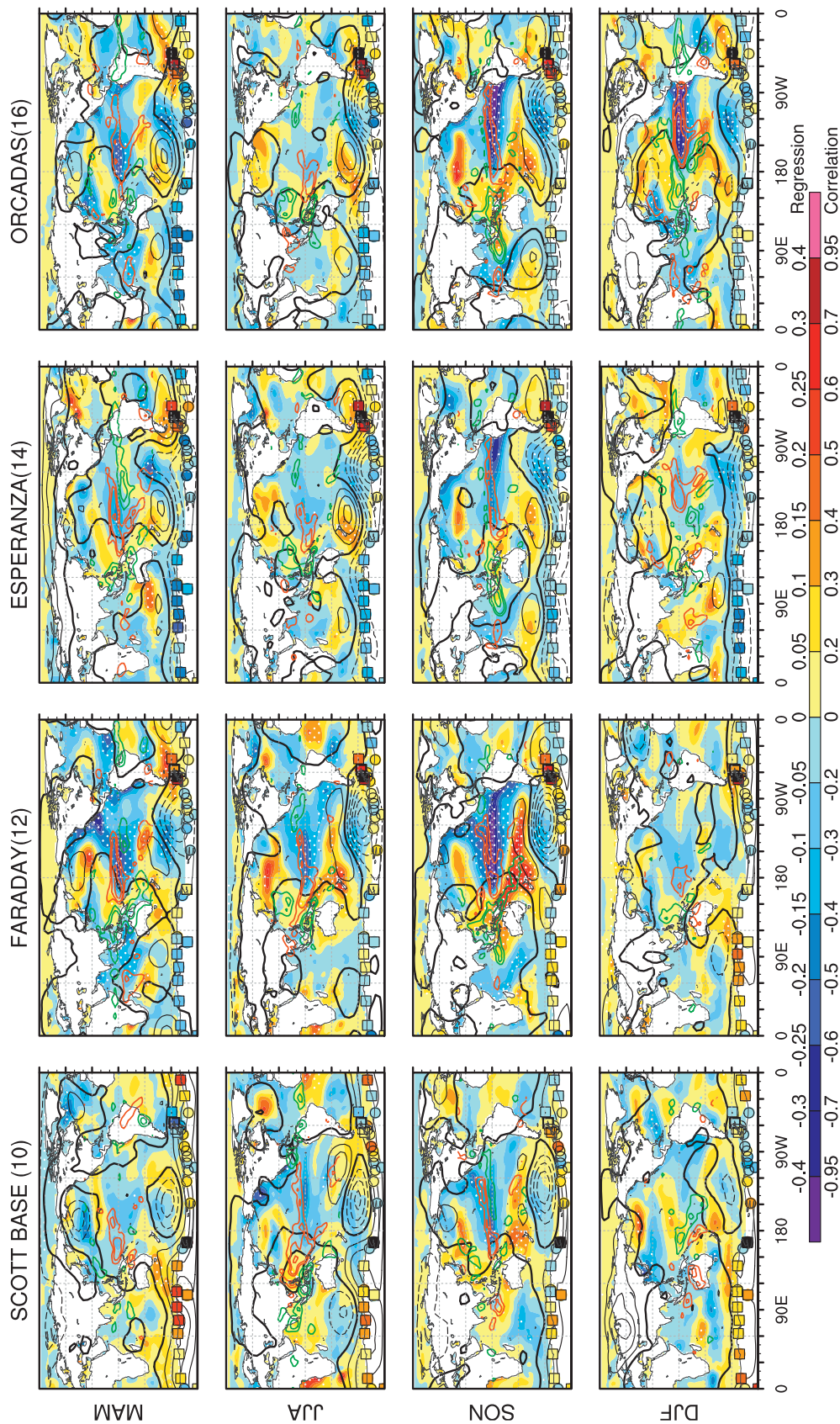


FIG. 4. As in Fig. 3, but for seasonal mean anomalies of SST, SLP, and precipitation regressed upon Antarctic station SATs at (left to right) Scott Base and three locations in the Antarctic Peninsula region (locations marked by solid black square). Also shown are correlations (values according to bottom scale) of the single station with all other Antarctic stations (generally, 1958–2008; colored squares) and with the annual ice core records (generally 1958–99; colored circles). All time series were linearly detrended before computing the regression or correlation coefficients.

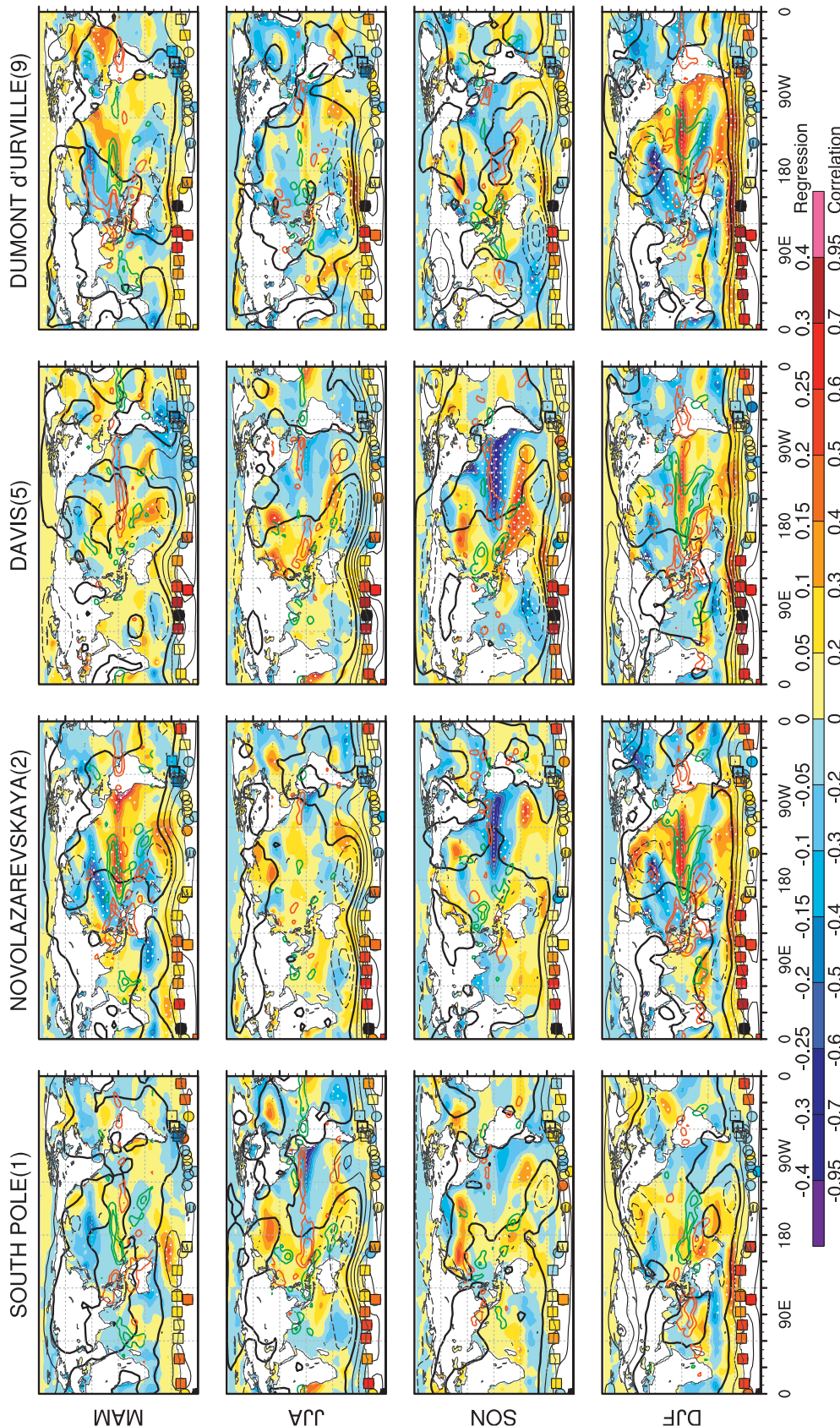


FIG. 5. As in Fig. 4, but for four station locations in the interior of Antarctica and coastal East Antarctica.

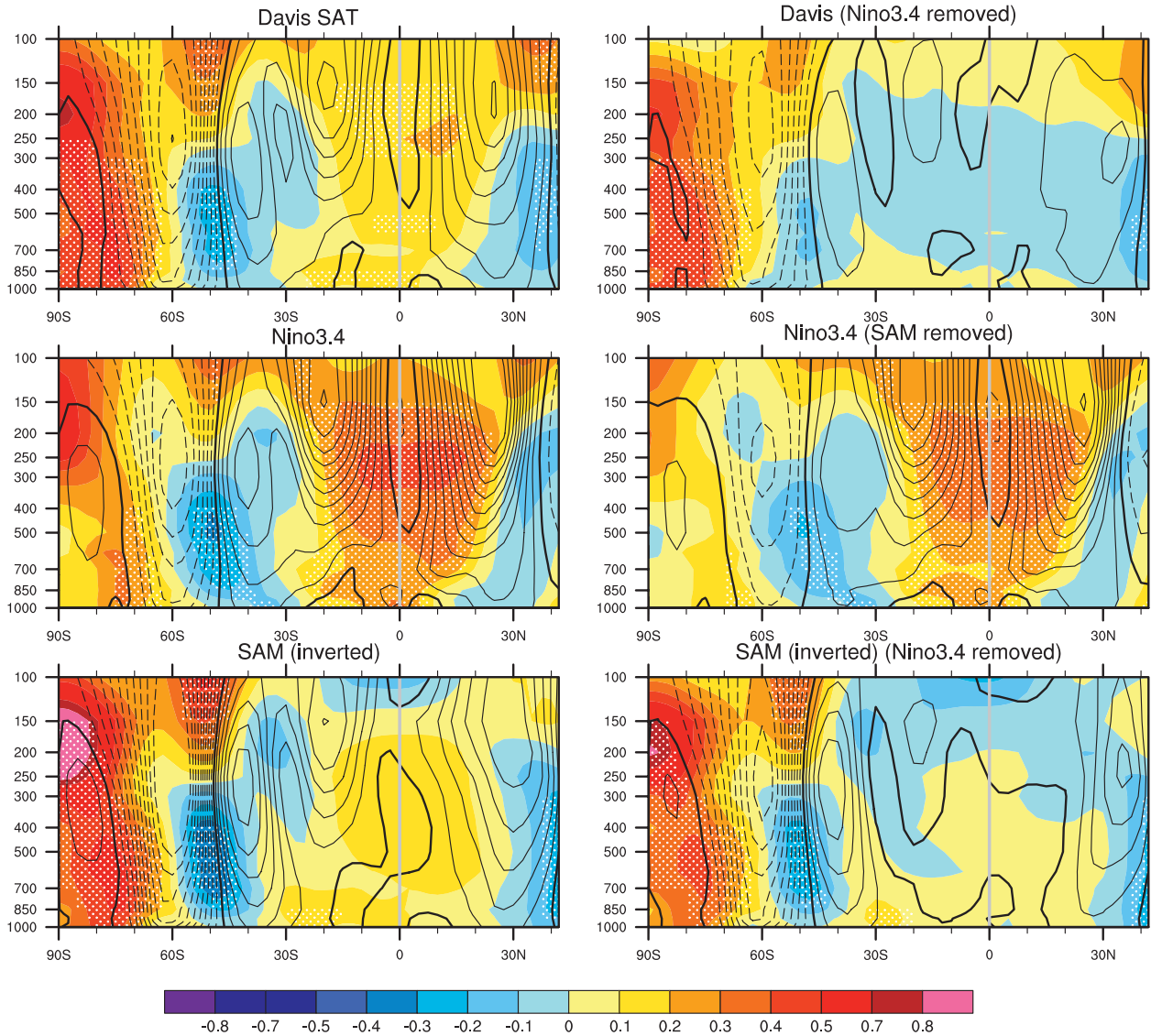


FIG. 6. Latitude–height cross sections showing (left) regressions of the austral summer (DJF) anomalies of NCEP2 zonal mean zonal wind (black contours, m s^{-1} per standard deviation; positive values solid and negative values dashed, interval of 0.2 m s^{-1}) and NCEP2 zonal mean temperature (colors; white stippling indicates values of at least the 95% significance level) upon the Davis station (top) temperature record, (middle) the Niño-3.4 index, and (bottom) the SAM index (sign inverted). (right) Regressions use the same indices but the Niño-3.4 variance has been removed from the NCEP2 anomalies for the Davis and SAM regressions, while the SAM variance has been removed for the Niño-3.4 regression. All time series were linearly detrended before computing the regression coefficients, and the period is 1979–2008.

Antarctica? We explore this question in Fig. 6, which compares the regressions of zonal mean zonal wind and temperature anomalies upon the Davis station record (representative of coastal East Antarctica) with those using the Niño-3.4 SST index (chosen instead of the SOI to more directly represent tropical heating–cooling) and the inverted SAM index. An immediate impression is the close resemblance of the three patterns. In the SH, all show a strengthening of zonal winds on the equatorward side of the subtropical jet, weakening of zonal winds on the poleward side of the jet, warming in the tropics and

poleward of $\sim 60^\circ\text{S}$, and cooling in the lower troposphere centered at $\sim 50^\circ\text{S}$. These anomalies are almost exactly as described by Seager et al. (2003) and L'Heureux and Thompson (2006). As in L'Heureux and Thompson (2006), we find that this pattern has a distinct seasonal occurrence confined to DJF.

To further explore the austral summer pattern, we show regressions with the Niño-3.4 variance linearly removed from the Davis and SAM records and the SAM variance removed from the Niño-3.4 index, in the right-hand column on Fig. 6. If the SAM variance is removed

TABLE 2. Correlations of 8-yr high-passed time series associated with the regressions in Fig. 7. Boldface values are statistically significant at the 95% confidence level or above.

	SOI SON	SOI DJF	SAM SON	SAM DJF
Faraday	0.43	-0.04	-0.18	-0.42
Davis	0.22	-0.43	-0.48	-0.74
SAM	0.10	0.38		

from the Niño-3.4 index, then the weakening of the SH subtropical jet is much less pronounced than for the original Niño-3.4 index. Removing the Niño-3.4 variance from the data, the tropical anomalies associated with the Davis and SAM records weaken considerably. For the SAM, the DJF regression with the Niño-3.4 variance removed resembles the SAM regressions in other seasons (not shown). This suggests that the SAM response to ENSO variability is only significant in DJF and supports the arguments of L'Heureux and Thompson (2006), that most of the extratropical SH response to ENSO projects onto the SAM. As a corollary, temperature anomalies at Davis are largely explained by the response of the SAM to ENSO. This explains the one-point regression maps in Fig. 5, which show correlations of temperature anomalies at East Antarctic coastal stations with SST and rainfall anomalies in the tropics, but no obvious signature of a Rossby wave train in the atmospheric circulation.

d. Timescale characteristics

To highlight the interannual time scales and seasons for which the Antarctic–tropical linkages are most pronounced, we apply an 8-yr high-pass filter to the seasonally stratified data. The high-pass filter is the Lanczos type using nine weights (Duchon 1979). Table 2 displays correlations of the filtered time series, using Faraday and Davis as representative records for the Antarctic Peninsula and coastal East Antarctica, respectively. In both SON and DJF, the Davis record is significantly correlated ($p < 0.05$) with the SAM ($r = -0.48$ and -0.74 , respectively). However, in DJF the Davis record also exhibits significant correlation with the SOI ($r = -0.43$). Consistently, the SAM and the SOI have a significant positive correlation in DJF ($r = 0.38$). The Faraday record has a significant correlation with the SOI in SON only ($r = 0.43$). In summary, in the austral spring, about 20% of the temporal variance in the Antarctic Peninsula region is linearly related to variations in the SOI, and in the austral summer, about 20% of the variance at East Antarctic coastal stations is linearly related to variations in the SOI.

We present the spatial patterns corresponding to the filtered time series in Fig. 7, comparing regressions using the SOI and the SAM index with regressions using the

Davis and Faraday records. This summarizes the key regional and seasonal aspects of the Antarctic–tropical linkages in the observational records, and suggests a fit to the mechanisms discussed in recent work. Essentially, the Faraday record exhibits a clear correspondence with ENSO variability in the austral spring. The rainfall, SST, and SLP patterns associated with anomalies at Faraday closely resemble those associated with the SOI, especially south of about 30°S. The prevalence of this linkage in spring is consistent with the seasonality of the SH Rossby wave source as defined by Jin and Kirtman (2009) and with the seasonality of the strength of the PSA wave train (Mo 2000; Trenberth and Caron 2000).

The spring ENSO teleconnection exhibits a modest impact in East Antarctica, as suggested by the resemblance of the regression patterns based on the SOI and Davis records (Fig. 7). However, the correlation of the Davis record with the SOI in spring ($r = 0.22$) is low and not statistically significant. In austral summer, Faraday SAT anomalies exhibit relationships with SST anomalies near the Antarctic Peninsula but not with remote SST anomalies in the tropics. At the same time, significant correlations develop between ENSO variability, the SAM, and East Antarctic temperature anomalies. This summer linkage cannot be explained by Rossby waves, but instead is consistent with the projection of ENSO variability onto the SAM.

e. Tropical linkages in ice cores

To provide a direct comparison to our analyses based on the Antarctic station data, we select eight of the ice core records described previously and compute one-point regression maps analogous to the maps using station data. Results are displayed in Fig. 8 for Gomez and three records from East Antarctica, and in Fig. 9 for four records from the West Antarctic Ice Sheet. To emphasize the interannual ENSO frequencies, the records are filtered with the 8-yr high-pass filter described above for the 1958–99 period.

Despite the annual resolution of the ice core records, the seasonal one-point regression maps based on these data tell a similar story to those based on the seasonally stratified station data. In Fig. 8, Gomez and Talos Dome records are associated with SLP anomalies in the South Pacific of the opposite sign. The amplitudes are largest in SON, consistent with the station data. The tropical SST pattern linearly related to positive isotopic anomalies at Gomez closely resembles the pattern related to the relatively close Faraday SAT record in SON. Rainfall anomalies are less evident because of the limited temporal overlap between the rainfall records and the Gomez record, which ends in 1980. Increased isotopic values at Talos Dome occur in association with

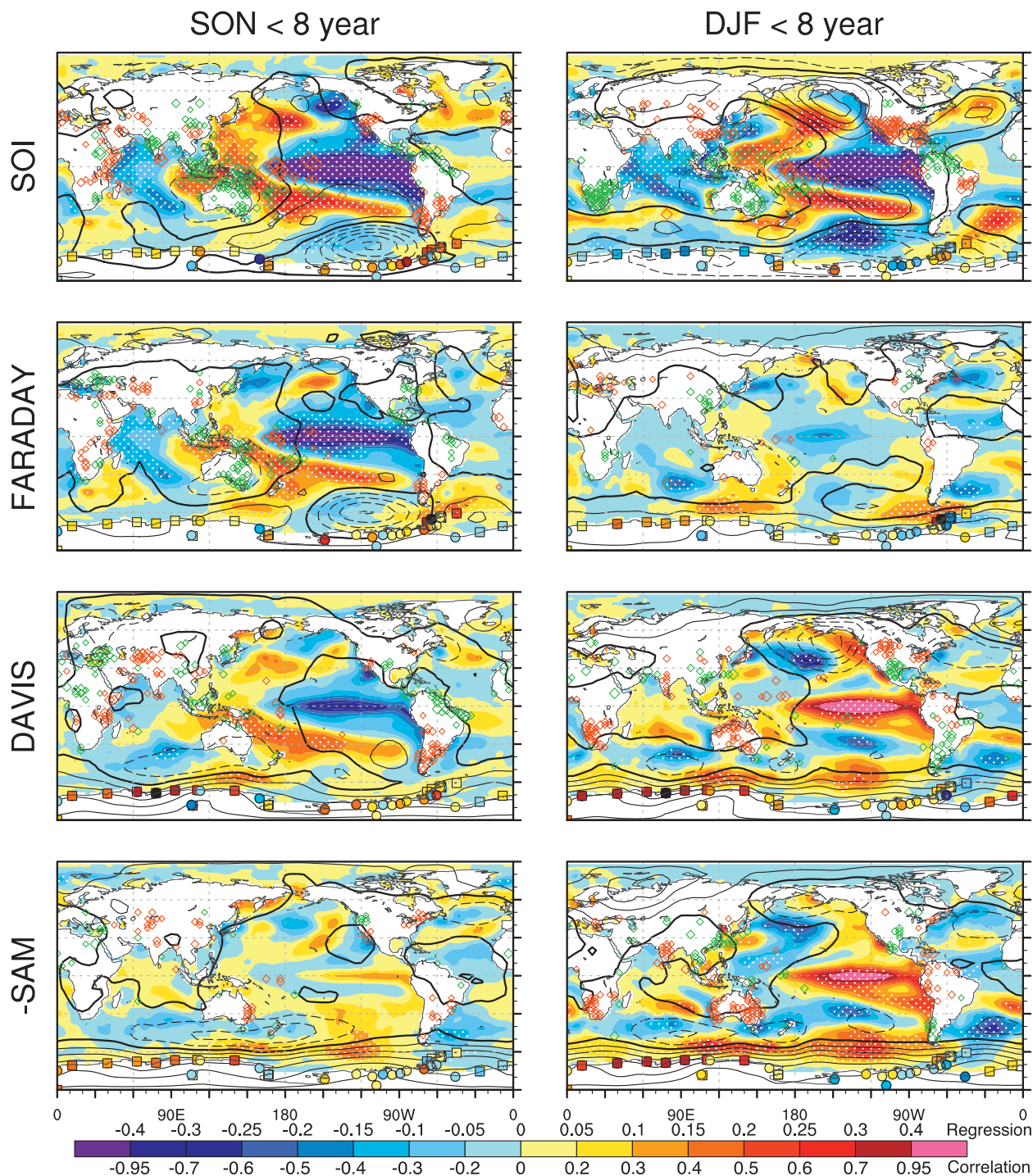


FIG. 7. Regressions of (left) SON and (right) DJF seasonal mean anomalies of SST (1958–2008; gridded colors, $^{\circ}\text{C}$ per standard deviation; white stippling indicates values of at least the 95% significance level) and SLP (1958–2008; black contours, hPa per standard deviation; positive values solid and negative values dashed, interval of 0.4 hPa) on corresponding seasonal mean (top to bottom) SOI, Faraday, Davis, and SAM time series. Also shown are correlations of the indices with Hulme et al. (1998) precipitation (generally, 1958–98; green diamonds positive values and orange diamonds negative values, scaled to the size of the correlation coefficient. Smallest size corresponds to values of -0.3 or 0.3 . Largest negative value is -0.93 ; largest positive value is 0.79 . No values between -0.30 and 0.30 are shown. A minimum overlap of 20 yr is required to show the precipitation correlations). In addition, the correlations of the index or single station with all other Antarctic stations (generally, 1958–2008; colored squares) and with the annual ice core records (generally 1958–99; colored circles) are shown. An 8-yr high-pass filter was applied to the seasonal mean Faraday, Davis, SAM, and SOI records as well as the Antarctic station and ice core records. All time series were linearly detrended before computing the regression or correlation coefficients.

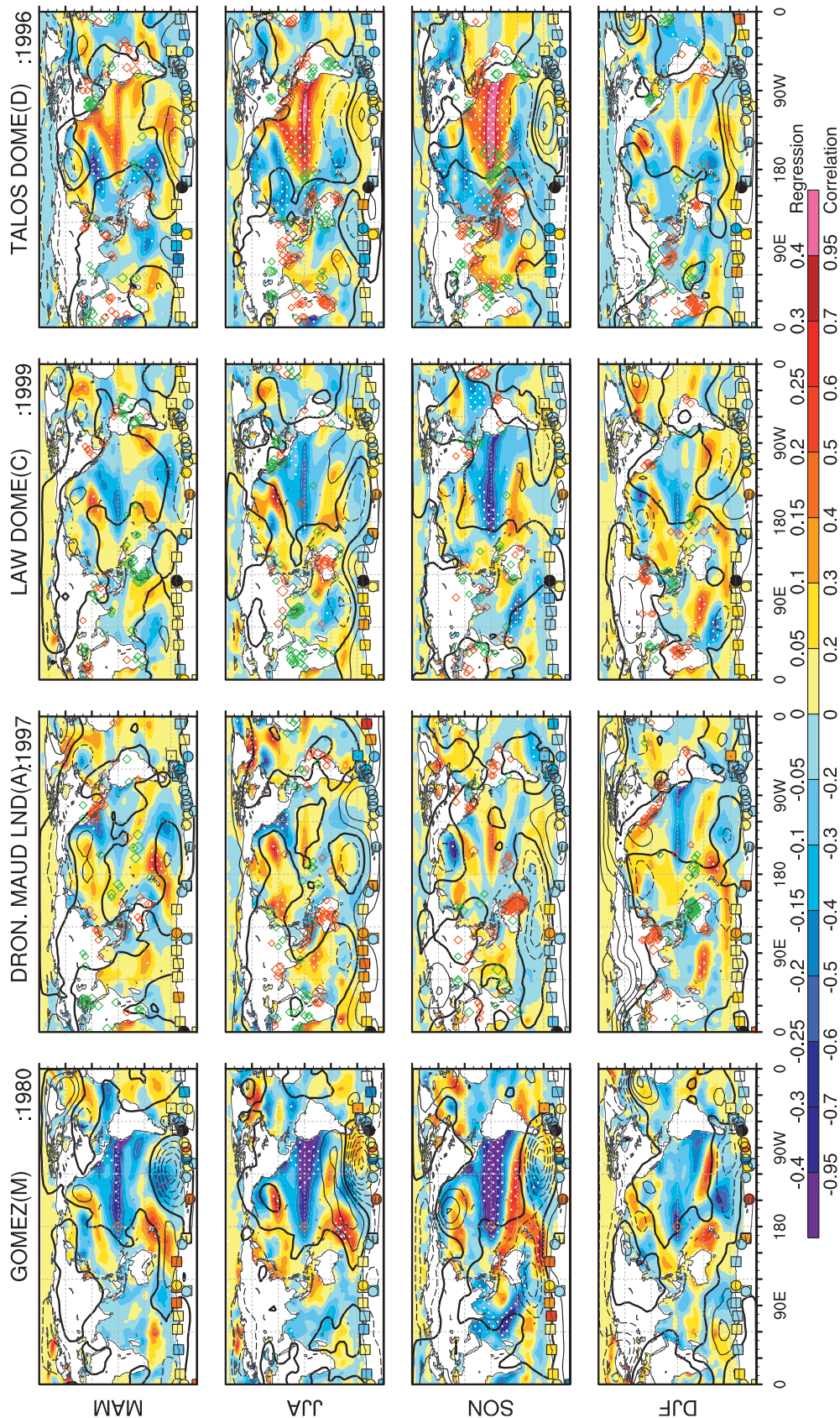


FIG. 8. Seasonal mean anomalies of SST, SLP, and precipitation regressed on annual mean anomalies of four Antarctic ice core records (locations indicated by solid black circles and names at the top of each column). SST, SLP, and precipitation fields are contoured as in Fig. 7. For the precipitation correlations, the largest positive value is $r = 0.74$ and the largest negative values is $r = -0.73$. Also shown are correlations of the ice core record with the Antarctic stations (generally, 1958–99; colored squares) and with the entire annual ice core records (generally 1958–99; colored circles). All time series were linearly detrended before computing the regression or correlation coefficients. Additionally, the ice core records were filtered with an 8-yr high-pass filter and then restandardized.

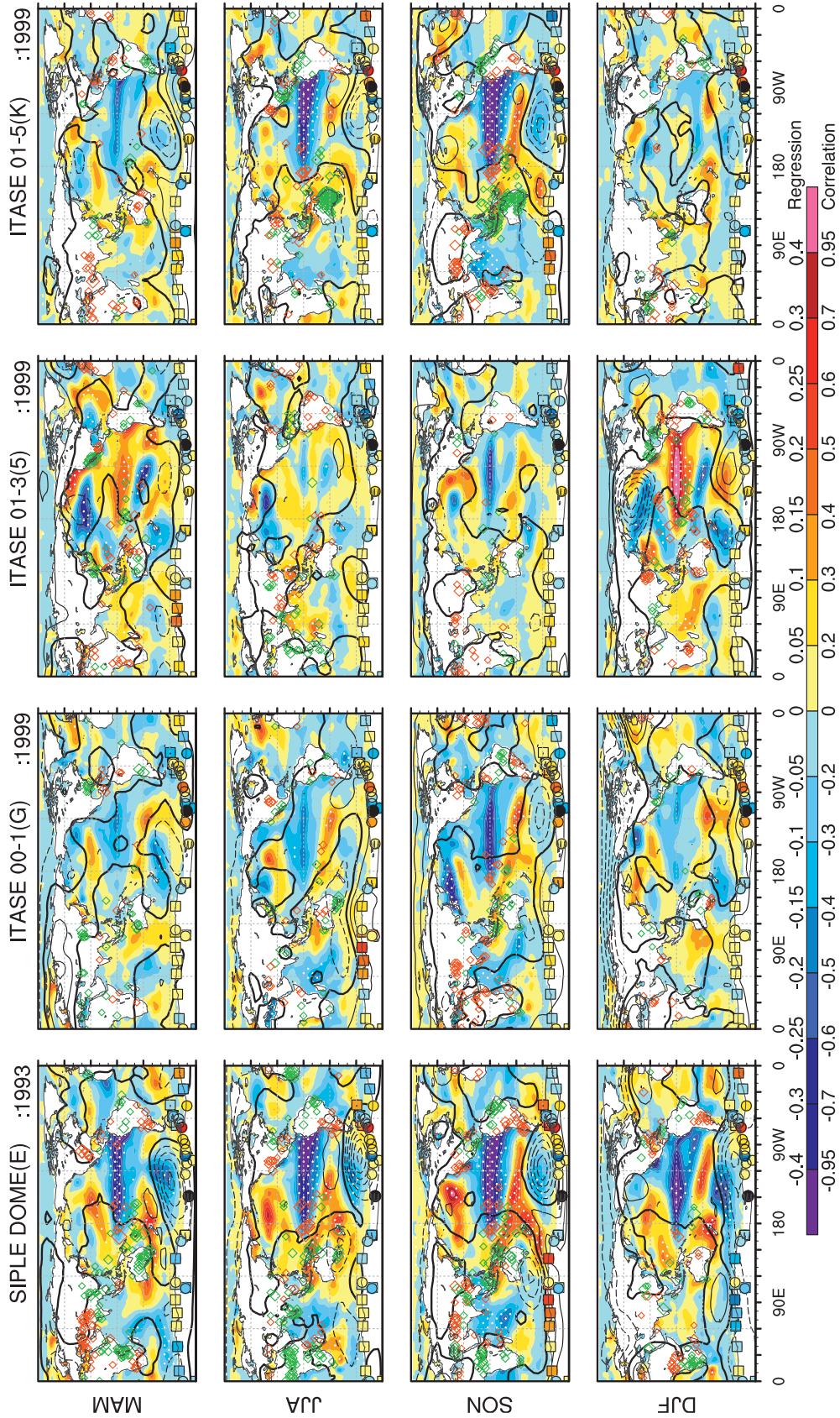


FIG. 9. As in Fig. 8, but for four ice core records from the West Antarctic Ice Sheet.

anticyclonic circulation anomalies in the Amundsen, Bellingshausen, and Ross Seas, which are consistent with a Rossby wave response to increased SSTs and rainfall in the central equatorial Pacific. This is also consistent with back-trajectory analysis for Talos Dome, which reveals that a large component of the annual accumulation comes from moisture transported from the Pacific sector during blocking events (Scarchilli et al. 2011; Masson-Delmotte et al. 2011).

Unlike Talos Dome, other records from East Antarctica, Dronning Maud Land, and Law Dome do not show clear teleconnection patterns. This suggests limited prospects for resolving the SAM component of the ENSO response in the high-latitude SH in DJF. This may be due to the short seasonal window during which this mechanism operates. As illustrated in Fig. 3, the PSA pattern associated with the SOI exists through much of the year, while the SAM's association with tropical variability is only pronounced in DJF. An ice core record, which integrates climatic conditions throughout the year and naturally smoothes short-lived, high-frequency signals, would not have fidelity in resolving a seasonal teleconnection like the SAM response in austral summer. Consideration of the seasonality of snow deposition rates, as well as the seasonality and locations of moisture sources (e.g., Scarchilli et al. 2011), further compounds the problem.

In Fig. 9, which shows results from West Antarctica, ice cores from Siple Dome and ITASE 01–5 show similar teleconnection patterns to Gomez, while the ITASE 00–1 and ITASE 01–3 patterns are rather noisy. The ITASE 01–5 site is closest to Gomez and sits in a relatively high deposition area (Fig. 1), while the ITASE 01–3 and 00–1 sites are farther away and have lower deposition rates. They are also located approximately in the middle of the Antarctic dipole region (e.g., Bromwich et al. 2004), so there is a high likelihood of nonstationarity in the strength and sign of ENSO signals in this region, a point explored by Gregory and Noone (2008).

Why do the cores from sites ITASE 01–5, Gomez, and Siple station (not shown) show such clear SLP patterns? Not only are the sites in relatively high snow accumulation areas and well located with respect to the PSA wave train but there is additional evidence that the seasonality of snow accumulation may align with the seasonality of the ENSO signal in this region. Studies of circulation and precipitation regimes in atmospheric models and reanalysis fields lend credibility to this idea. Specifically, as noted by Marshall (2009), the wave-3 nature of the annual surface mass balance coincides with the climatological wave-3 pattern of low pressure centers in the circumpolar trough (Bromwich and Wang 2008). The deepest low pressure center occurs near 130°W, with the largest surface mass balance to the east. Secondary closed

lows are evident near 25° and 110°E, consistent with surface mass balance maxima at ~50° and ~130°E. From austral winter to summer, the low pressure centers migrate: the “Amundsen Sea” low center moves from ~150°W off the coast of Marie Byrd Land to the Bellingshausen Sea (see Fig. 2 in Bromwich and Wang 2008). This implies more accumulation in West Antarctica from roughly 90° to 70°W in austral spring and summer than at other times of the year. Nicolas and Bromwich (2011) presented a limited-period dataset that shows the greatest accumulation in Ellsworth Land in the austral spring, consistent with the seasonality of the regression patterns of cores Gomez and ITASE 01–5. High-quality, seasonally resolved, long-term accumulation datasets are needed to develop this idea further.

4. Summary and discussion

Our results detail a variety of physical evidence that collectively illustrates the impacts of tropical climate variability on the climate of the Antarctic. Our results also confirm and extend evidence for two mechanisms whereby tropical Pacific ENSO signals reach the Antarctic. The first mechanism, involving the PSA pattern and its interpretation as a Rossby wave train propagating from the tropics to the high latitudes, has been discussed in numerous studies (e.g., Karoly 1989; Mo and Higgins 1998; Mo 2000; Jin and Kirtman 2009). Impacts of the PSA have been previously summarized by Turner (2004) and Russell and McGregor (2010). However, these studies have paid little attention to seasonality or have emphasized only a single season, for example, winter in Mo and Higgins (1998). Regressions using the SOI demonstrate that the maximum amplitude of the circulation anomaly in the southeastern South Pacific occurs during austral spring. Supporting evidence includes regressions using Faraday station data from the western Antarctic Peninsula, as well as nearby ice cores Gomez and ITASE 01–5. All of these results illustrate the strong seasonality of the PSA teleconnection, and significant linkages to tropical SST and precipitation anomalies. These linkages, however, disappear in the austral summer at the peak of the ENSO cycle, and are relatively weak during the austral autumn and winter preceding the ENSO peak. Physical explanations for this seasonality have been provided only recently (Jin and Kirtman 2009, 2010).

The second mechanism involving the projection of ENSO variability onto the SAM is a relatively new area of study (Seager et al. 2003; L'Heureux and Thompson 2006; Fogt and Bromwich 2006; Fogt et al. 2011). This mechanism also has a distinct seasonality, evident primarily in the austral summer, for reasons that have not been fully explored. The seasonality may simply reflect the

maximum amplitude of tropical heating associated with the ENSO cycle (L'Heureux and Thompson 2006), but it likely also involves seasonal characteristics of the extratropical atmosphere (Jin and Kirtman 2009, 2010; Trenberth et al. 1998). In the austral summer, our results show statistically significant correlations between ENSO variability and temperature anomalies at East Antarctic coastal stations. One-point regression maps show clear ENSO signatures in the tropics: Associated with positive temperature anomalies at Davis, there are increased rainfall and positive SST anomalies in the eastern Pacific, and decreased rainfall and negative SST anomalies in the western Pacific, consistent with El Niño conditions. As discussed in other studies, the mechanism involves the combination of thermally driven zonal wind anomalies in the tropics and subtropics, and eddy-driven zonal wind anomalies in the mid- and high latitudes (Seager et al. 2003; L'Heureux and Thompson 2006; Fogt et al. 2011; Gong et al. 2010). Our regressions using the Davis station data (Fig. 6) illustrate the impacts of this mechanism and confirm the seasonality suggested by L'Heureux and Thompson (2006).

The disappearance of the tropical teleconnection at Faraday from austral spring to summer is an apparent paradox, as it might be expected that in spring SAT anomalies at Faraday are associated with the PSA pattern and in summer they are associated with the SAM. However, a number of observational and modeling studies have shown that anomalous northerly or northwesterly winds (associated with the PSA) usually mean relatively warm conditions at Faraday, but anomalous westerly winds do not always show a significant SAT response. Marshall et al. (2006) observed that in DJF, SAT anomalies are weakly negatively correlated with the SAM, partly due to a northerly component to the winds. The authors also found that anomalous westerlies during positive SAM phases, which would also be expected to favor warm air advection, tend to be focused farther north on the Antarctic Peninsula than Faraday station. In addition, the positive SAM phase is associated with less blocking on the western side of the Antarctic Peninsula and more flow-over conditions to the eastern side, where adiabatic compression leads to warming. The observational analyses of Marshall et al. (2006) was followed up and generally confirmed by the high-resolution modeling study of van Lipzig et al. (2008). These studies, which highlight the role of the complex orography around the Antarctic Peninsula in determining the SAT response to atmospheric circulation anomalies, help to explain the association of SAT anomalies at Faraday with the tropical teleconnection patterns. The same studies also point out that the positive SAM phase (increased westerlies) is associated with

warm anomalies at stations to the north and east of Faraday, Esperanza, and Orcadas, consistent with our regression maps (e.g., Fig. 4).

The characterization of Antarctic climate variability and its tropical linkages on the interannual time scale likely relates as well to the mechanisms that drive decadal climate variability in Antarctica. It has long been recognized that large decadal variability exists in Antarctic climate (e.g., Chapman and Walsh 2007), but what controls this variability is not well known. Using extended versions of the ice core records discussed here, we are currently evaluating Antarctic decadal climate variability and its tropical linkages (Okumura et al. 2012). Better understanding of these linkages could inform both seasonal and longer-term predictions of Antarctic climate. The prevalence of ENSO signals in the austral spring and summer suggests a potential for seasonal predictability, at the time of year when seasonal forecasts would be very useful to Antarctic logistical operations. On the longer time-scale perspective, Schneider et al. (2012) assessed Antarctic temperature trends, finding the most significant trend on the continent to be the warming of West Antarctica in the austral spring for 1979–2009. The warming trend is related to a strong cyclonic atmospheric circulation trend in the South Pacific, which is consistent with intensified Rossby wave activity driven by trends in low-latitude SSTs. If tropical SST trends and low-frequency phenomena, such as the Pacific decadal oscillation, (Mantua et al. 1997) could be predicted, then this implies a new potential for Antarctic climate predictability, in addition to ozone hole trajectories (e.g., Perlwitz et al. 2008; Son et al. 2009). More detailed statistical and modeling studies will be necessary to test these ideas further.

Acknowledgments. D. P. Schneider and Y. Okumura were supported the National Science Foundation, Office of Polar Programs (Grant 0838871). We thank three anonymous reviewers for their constructive comments, which led to numerous improvements to the paper.

REFERENCES

- Adler, R. F., and Coauthors, 2003: The Version-2 Global Precipitation Climatology Project (GPCP) monthly precipitation analysis (1979–present). *J. Hydrometeorol.*, **4**, 1147–1167.
- Allan, R., and T. Ansell, 2006: A new globally complete monthly historical gridded mean sea level pressure dataset (HadSLP2): 1850–2004. *J. Climate*, **19**, 5816–5842.
- Bals-Elsholz, T., E. Atallah, L. Bosart, T. Wasula, M. Cempa, and A. Lupo, 2001: The wintertime Southern Hemisphere split jet: Structure, variability, and evolution. *J. Climate*, **14**, 4191–4215.
- Bromwich, D. H., and S. H. Wang, 2008: A review of the temporal and spatial variability of the Arctic and Antarctic atmospheric circulations based upon ERA-40. *Dyn. Atmos. Oceans*, **44**, 213–243.

- , A. N. Rogers, P. Kållberg, R. I. Cullather, J. W. C. White, and K. J. Kreutz, 2000: ECMWF analyses and reanalyses depiction of ENSO signal in Antarctic precipitation. *J. Climate*, **13**, 1406–1420.
- , A. J. Monaghan, and Z. C. Guo, 2004: Modeling the ENSO modulation of Antarctic climate in the late 1990s with the polar MM5. *J. Climate*, **17**, 109–132.
- Cai, W. J., and I. G. Watterson, 2002: Modes of interannual variability of the Southern Hemisphere circulation simulated by the CSIRO climate model. *J. Climate*, **15**, 1159–1174.
- Carvalho, L. M. V., C. Jones, and T. Ambrizzi, 2005: Opposite phases of the Antarctic Oscillation and relationships with intraseasonal to interannual activity in the tropics during the austral summer. *J. Climate*, **18**, 702–718.
- Chapman, W. L., and J. E. Walsh, 2007: A synthesis of Antarctic temperatures. *J. Climate*, **20**, 4096–4117.
- Ciasto, L. M., and D. W. J. Thompson, 2008: Observations of large-scale ocean–atmosphere interaction in the Southern Hemisphere. *J. Climate*, **21**, 1244–1259.
- Cullather, R. I., D. H. Bromwich, and M. L. VanWoert, 1996: Interannual variations in Antarctic precipitation related to El Niño–Southern Oscillation. *J. Geophys. Res.*, **101**, 19 109–19 118.
- Deser, C., A. Capotondi, R. Saravanan, and A. S. Phillips, 2006: Tropical Pacific and Atlantic climate variability in CCSM3. *J. Climate*, **19**, 2451–2481.
- , M. A. Alexander, S.-P. Xie, and A. S. Phillips, 2010: Sea surface temperature variability: Patterns and mechanisms. *Annu. Rev. Mar. Sci.*, **2**, 115–143, doi:10.1146/annurev-marine-120408-151453.
- Ding, Q., E. J. Steig, D. S. Battisti, and M. Kuttel, 2011: Winter warming in West Antarctica caused by central tropical Pacific warming. *Nat. Geosci.*, **4**, 398–403, doi:10.1038/ngeo1129.
- Divine, D. V., and Coauthors, 2009: Tropical Pacific–high latitude South Atlantic teleconnections as seen in $\delta^{18}\text{O}$ variability in Antarctic coastal ice cores. *J. Geophys. Res.*, **114**, D11112, doi:10.1029/2008JD010475.
- Duchon, C. E., 1979: Lanczos filtering in one and two dimensions. *J. Appl. Meteor.*, **18**, 1016–1102.
- Fogt, R. L., and D. H. Bromwich, 2006: Decadal variability of the ENSO teleconnection to the high-latitude South Pacific governed by coupling with the southern annular mode. *J. Climate*, **19**, 979–997.
- , —, K. M. Hines, 2011: Understanding the SAM influence on the South Pacific ENSO teleconnection. *Climate Dyn.*, **36**, 1555–1576, doi:10.1007/s00382-010-0905-0.
- Ghil, M., and K. Mo, 1991: Intraseasonal oscillations in the global atmosphere. Part I: Northern Hemisphere and tropics. *J. Atmos. Sci.*, **48**, 752–779.
- Gong, T., S. B. Feldstein, and D. Luo, 2010: The impact of ENSO on wave breaking and southern annular mode events. *J. Atmos. Sci.*, **67**, 2854–2870.
- Gregory, S., and D. Noone, 2008: Variability in the teleconnection between the El Niño–Southern Oscillation and West Antarctic climate deduced from West Antarctic ice core isotope records. *J. Geophys. Res.*, **113**, D17110, doi:10.1029/2007JD009107.
- Hulme, M., T. J. Osborn, and T. C. Johns, 1998: Precipitation sensitivity to global warming: Comparison of observations with HadCM2 simulations. *Geophys. Res. Lett.*, **25**, 3379–3382.
- Ichiyanagi, K., A. Numaguti, and K. Kato, 2002: Interannual variation of stable isotopes in Antarctic precipitation in response to El Niño–Southern Oscillation. *Geophys. Res. Lett.*, **29**, 1001, doi:10.1029/2000GL012815.
- Jin, D., and B. P. Kirtman, 2009: Why the Southern Hemisphere ENSO responses lead ENSO. *J. Geophys. Res.*, **114**, D23101, doi:10.1029/2009JD012657.
- , and —, 2010: How the annual cycle affects the extratropical response to ENSO. *J. Geophys. Res.*, **115**, D06102, doi:10.1029/2009JD012660.
- Kanamitsu, M., W. Ebisuzaki, J. Woollen, S.-K. Yang, J. J. Hnilo, M. Fiorino, and G. L. Potter, 2002: NCEP–DOE AMIP-II Reanalysis (R-2). *Bull. Amer. Meteor. Soc.*, **83**, 1631–1643.
- Karoly, D. J., 1989: Southern Hemisphere circulation features associated with El Niño–Southern Oscillation events. *J. Climate*, **2**, 1239–1252.
- Kwok, R., and J. C. Comiso, 2002: Spatial patterns of variability in Antarctic surface temperature: Connections to the Southern Hemisphere annular mode and the Southern Oscillation. *Geophys. Res. Lett.*, **29**, 1705, doi:10.1029/2002GL015415.
- L’Heureux, M. L., and D. W. J. Thompson, 2006: Observed relationships between the El Niño–Southern Oscillation and the extratropical zonal-mean circulation. *J. Climate*, **19**, 276–287.
- Limpasuvan, V., and D. L. Hartmann, 2000: Wave-maintained annular modes of climate variability. *J. Climate*, **13**, 4414–4429.
- Mantua, N. J., S. R. Hare, Y. Zhang, J. M. Wallace, and R. C. Francis, 1997: A Pacific interdecadal climate oscillation with impacts on salmon production. *Bull. Amer. Meteor. Soc.*, **78**, 1069–1079.
- Marshall, G. J., 2003: Trends in the southern annular mode from observations and reanalyses. *J. Climate*, **16**, 4134–4143.
- , 2009: On the annual and semiannual cycles of precipitation across Antarctica. *Int. J. Climatol.*, **29**, 2298–2308.
- , A. Orr, N. P. M. van Lipzig, and J. C. King, 2006: The impact of a changing Southern Hemisphere annular mode on Antarctic Peninsula summer temperatures. *J. Climate*, **19**, 5388–5404.
- Masson-Delmotte, V., and Coauthors, 2008: A review of Antarctic surface snow isotopic composition: Observations, atmospheric circulation, and isotopic modeling. *J. Climate*, **21**, 3359–3387.
- , and Coauthors, 2011: A comparison of the present and last interglacial periods in six Antarctic ice cores. *Climate Past*, **7**, 397–423.
- Mo, K. C., 2000: Relationships between low-frequency variability in the Southern Hemisphere and sea surface temperature anomalies. *J. Climate*, **13**, 3599–3610.
- , and G. H. White, 1985: Teleconnections in the Southern Hemisphere. *Mon. Wea. Rev.*, **113**, 22–37.
- , and R. W. Higgins, 1998: The Pacific–South American modes and tropical convection during the Southern Hemisphere winter. *Mon. Wea. Rev.*, **126**, 1581–1596.
- , and J. N. Paegle, 2001: The Pacific–South American modes and their downstream effects. *Int. J. Climatol.*, **21**, 1211–1229.
- Naik, S. S., M. Thamban, C. M. Laluraj, B. L. Redkar, and A. Chaturvedi, 2010: A century of climate variability in central Dronning Maud Land, East Antarctica, and its relation to southern annular mode and El Niño–Southern Oscillation. *J. Geophys. Res.*, **115**, D16102, doi:10.1029/2009JD013268.
- Neelin, J. D., D. S. Battisti, A. C. Hirst, F.-F. Jin, Y. Wakata, T. Yamagata, and S. E. Zebiak, 1998: ENSO theory. *J. Geophys. Res.*, **103**, 14 261–14 290.
- Nicolas, J. P., and D. H. Bromwich, 2011: Climate of West Antarctica and influence of marine air intrusions. *J. Climate*, **24**, 49–67.
- Okumura, Y. M., D. Schneider, C. Deser, and R. Wilson, 2012: Decadal–interdecadal climate variability over Antarctica and

- linkages to the tropics: Analysis of ice core, instrumental, and tropical proxy data. *J. Climate*, in press.
- Peel, D. A., R. Mulvaney, and B. M. Davison, 1988: Stable-isotope/air-temperature relationships in ice cores from Dolleman Island and the Palmer Land Plateau, Antarctic Peninsula. *Ann. Glaciol.*, **10**, 130–136.
- Perlwitz, J., S. Pawson, R. L. Fogt, J. E. Nielsen, and W. D. Neff, 2008: Impact of stratospheric ozone hole recovery on Antarctic climate. *Geophys. Res. Lett.*, **35**, L08714, doi:10.1029/2008GL033317.
- Renwick, J. A., 2002: Southern Hemisphere circulation and relations with sea ice and sea surface temperature. *J. Climate*, **15**, 3058–3068.
- Robertson, A. W., and C. R. Mechoso, 2003: Circulation regimes and low-frequency oscillations in the South Pacific sector. *Mon. Wea. Rev.*, **131**, 1566–1576.
- Russell, A., and G. R. McGregor, 2010: Southern Hemisphere atmospheric circulation: Impacts on Antarctic climate and reconstructions from Antarctic ice core data. *Climatic Change*, **99**, 155–192, doi:10.1007/s10584-009-9673-4.
- Savage, M. L., C. R. Stearns, and G. A. Weidner, 1988: The Southern Oscillation signal in Antarctica. Preprints, *Second Conf. on Polar Meteorology and Oceanography*, Madison, WI, Amer. Meteor. Soc., 141–144.
- Scarchilli, C., M. Frezzottu, and P. M. Ruti, 2011: Snow precipitation at four ice core sites in East Antarctica: Provenance, seasonality and blocking factors. *Climate Dyn.*, **37**, 2107–2125, doi:10.1007/s00382-010-0946-4.
- Schneider, D. P., and D. C. Noone, 2007: Spatial covariance of water isotope records in a global network of ice cores spanning twentieth-century climate change. *J. Geophys. Res.*, **112**, D18105, doi:10.1029/2007JD008652.
- , and E. J. Steig, 2008: Ice cores record significant 1940s Antarctic warmth related to tropical climate variability. *Proc. Natl. Acad. Sci. USA*, **105**, 12 154–12 158, doi:10.1073/pnas.0803627105.
- , —, and J. C. Comiso, 2004: Recent climate variability in Antarctica from satellite-derived temperature data. *J. Climate*, **17**, 1569–1583.
- , —, T. D. van Ommen, D. A. Dixon, P. A. Mayewski, J. M. Jones, and C. M. Bitz, 2006: Antarctic temperatures over the past two centuries from ice cores. *Geophys. Res. Lett.*, **33**, L16707, doi:10.1029/2006GL027057.
- , C. Deser, Y. M. Okumura, 2012: An assessment and interpretation of the observed warming of West Antarctica in the austral spring. *Climate Dyn.*, **38**, 332–347, doi:10.1007/s00382-010-0985-x.
- Seager, R., N. Harnik, Y. Kushnir, W. Robinson, and J. Miller, 2003: Mechanisms of hemispherically symmetric climate variability. *J. Climate*, **16**, 2960–2978.
- , —, W. Robinson, Y. Kushnir, M. Ting, H.-P. Huang, and J. Velez, 2005: Mechanisms of ENSO-forcing of hemispherically symmetric precipitation variability. *Quart. J. Roy. Meteor. Soc.*, **131**, 1501–1527, doi:10.1256/qj.04.96.
- , N. Naik, M. Ting, M. A. Cane, N. Harnik, and Y. Kushnir, 2010: Adjustment of the atmospheric circulation to tropical Pacific SST anomalies: Variability of transient eddy propagation in the Pacific–North America sector. *Quart. J. Roy. Meteor. Soc.*, **136**, 277–296, doi:10.1002/qj.588.
- Smith, T. M., R. W. Reynolds, T. C. Peterson, and J. Lawrimore, 2008: Improvements to NOAA's historical merged land-ocean surface temperature analysis (1880–2006). *J. Climate*, **21**, 2283–2296.
- Son, S.-W., N. F. Tandon, L. M. Polvani, and D. W. Waugh, 2009: Ozone hole and Southern Hemisphere climate change. *Geophys. Res. Lett.*, **36**, L15705, doi:10.1029/2009GL038671.
- Steig, E. J., and Coauthors, 2005: High-resolution ice cores from USITASE (West Antarctica): Development and validation of chronologies and determination of precision and accuracy. *Ann. Glaciol.*, **41**, 77–84.
- , Q. Ding, D. S. Battisti, A. Jenkins, 2012: Tropical forcing of circumpolar deep water inflow and outlet glacier thinning in the Amundsen Sea Embayment, West Antarctica. *Ann. Glaciol.*, **53**, 19–28.
- Thompson, D. W. J., J. M. Wallace, and G. C. Hegerl, 2000: Annular modes in the extratropical circulation. Part I: Month-to-month variability. *J. Climate*, **13**, 1000–1016.
- Trenberth, K. E., 1975: A quasi-biennial standing wave in Southern Hemisphere and interrelations with sea surface temperature. *Quart. J. Roy. Meteor. Soc.*, **101**, 55–74.
- , 1984: Signal versus noise in the Southern Oscillation. *Mon. Wea. Rev.*, **112**, 326–332.
- , and J. Caron, 2000: The Southern Oscillation revisited: Sea level pressures, surface temperatures, and precipitation. *J. Climate*, **13**, 4358–4365.
- , G. W. Branstator, D. Karoly, A. Kumar, N.-C. Lau, and C. Ropelewski, 1998: Progress during TOGA in understanding and modeling global teleconnections associated with tropical sea surface temperatures. *J. Geophys. Res.*, **103**, 14 291–14 324.
- Turner, J., 2004: The El Niño–Southern Oscillation and Antarctica. *Int. J. Climatol.*, **24**, 1–31.
- , and Coauthors, 2004: The SCAR READER project: Toward a high-quality database of mean Antarctic meteorological observations. *J. Climate*, **17**, 2890–2898.
- van de Berg, W. J., M. R. van den Broeke, C. H. Reijmer, and E. van Meijgaard, 2006: Reassessment of the Antarctic surface mass balance using calibrated output of a regional atmospheric climate model. *J. Geophys. Res.*, **111**, D11104, doi:10.1029/2005JD006495.
- van Lipzig, N. P. M., G. J. Marshall, A. Orr, and J. C. King, 2008: The relationship between the Southern Hemisphere annular mode and Antarctic Peninsula summer temperatures: Analysis of a high-resolution model climatology. *J. Climate*, **21**, 1649–1668.
- Wallace, J. M., and D. S. Gutzler, 1981: Teleconnections in the geopotential height field during the Northern Hemisphere winter. *Mon. Wea. Rev.*, **109**, 784–812.
- Williams, L. N., S. Lee, and S. Son, 2007: Dynamics of the Southern Hemisphere spiral jet. *J. Atmos. Sci.*, **64**, 548–563.
- Yuan, X., and C. Li, 2008: Climate modes in southern high latitudes and their impacts on Antarctic sea ice. *J. Geophys. Res.*, **113**, C06S91, doi:10.1029/2006JC004067.
- , and D. G. Martinson, 2000: Antarctic sea ice extent variability and its global connectivity. *J. Climate*, **13**, 1697–1717.
- Zhang, Y., J. M. Wallace, and D. S. Battisti, 1997: ENSO-like interdecadal variability: 1900–93. *J. Climate*, **10**, 1004–1020.